

# High Performance MEMS Micro-Gyroscope

Sam Y. Bae, Ken J. Hayworth, Karl Y. Yee, Kirill Shcheglov, A. Dorian Challoner, Dean V. Wiberg  
Jet Propulsion Laboratory, California Institute of Technology  
E-mail: ybae@mail1.jpl.nasa.gov

## Abstract

This paper reports on JPL's on-going research into MEMS gyroscopes. [1-3] This paper will describe the gyroscope's fabrication-methods, a new 8-electrode layout developed to improve performance, and performance statistics of a batch of six gyroscopes (of the 8-electrode design) recently rate tested. Previously in our group, T. Tang and R. Gutierrez presented the results of their extensive use of ethylene diamine pyrocatechol (EDP) to deep-etch the inertial-sensitive resonators and post-supporting structures in a 4-electrode gyroscope design. Today, JPL is utilizing an in-house STS DRIE, replaced the old wet-etching steps. This has demonstrated superior precision in machining symmetry of the resonators, thus significantly reducing native rocking mode frequency-splits. A performance test of six gyros has shown an average, un-tuned, frequency split of 0.4% (11Hz split for rocking modes at 2.7KHz). The new JPL MEMS gyroscope has a unique 8-electrode layout, whose large electrodes can provide significant electrostatic softening of the resonator's springs. This allows matching of the Coriolis sensitive rocking modal frequencies to be improved from the native 0.4% to an average tuned frequency split of 0.02%. In separate tests, electrostatic tuning in the 8-electrode design has demonstrated the ability to match frequency-splits to within 10mHz, thus ensuring full degeneracy in even a very high Q device. In addition, a newly selected ceramic package-substrate has improved the device's dampening losses such that a mean Q of 28,000 was achieved in the six gyros tested. These Q's were measured via the ring-down time method. The improved fabrication development and other modifications described have led to the JPL's MEMS gyroscope achieving an average bias instability (Allan variance 1/f floor estimate) of 11degree/hr with best in the group being 2degree/hr. In an independent test, Honeywell Inc., reported one of our MEMS gyroscopes as achieving 1degree/hr bias instability flicker floor estimate measured at constant temperature.

## Introduction

A gyroscope is a commonly used sensor for measuring angular velocity. Although conventional rotating wheel, fiber optic, and ring-laser gyroscopes are dominant in many applications, their size, power-hungry mechanism, and cost limit their usage in a wider range of industries such as automobile, satellite, video game, and handheld positioning systems. However, the advent of MEMS machining technologies has made fabrications of miniature gyroscopes and their applications possible in that broader market. The JPL micro-gyroscope team has leveraged the available MEMS machining technologies and fabricated a gyroscope, 1) being several orders of magnitudes smaller than the conventional gyroscopes, thus as a byproduct, 2) consumes little power, and 3) manufactured in bulk which leads to lowering its cost and making it easily available in the market.

However, the MEMS gyroscope technology has not yet matured to the point that it meets the demands of high performance markets (roughly requiring a bias stability of less than 1degree/hr). In light of JPL's "faster, better, cheaper" space missions' and highest standard requirement for navigation sensors, the JPL MEMS team is focused on a sub-1degree/hr performance range goal.

## JPL's MEMS Gyroscope Principles

Figure 1 shows a sketch of JPL's MEMS gyroscope unit. The MEMS fabricated gyroscope consists of three parts: 1) a two degree-of-freedom resonating 4-leaf-clover, suspended by 4 T-springs at each edge, 2) a post providing the main inertial mass, running perpendicular to  $\theta_1$ - $\theta_2$  plane (hereon we abbreviate the first two units as "cloverleaf"), 3) an 8-electrodes baseplate that drives and senses the rocking motions of the cloverleaf (hereon called the "electrode-plate"), and 4) a simple 3mm thick square die having a drilled hole, this is attached below the electrode-plate, and

allows the protruded post to move freely (hereon called the “spacer”, not shown in Figure 1). The dimensions of an assembled micro-gyroscope are 9 x 9 x 6mm.

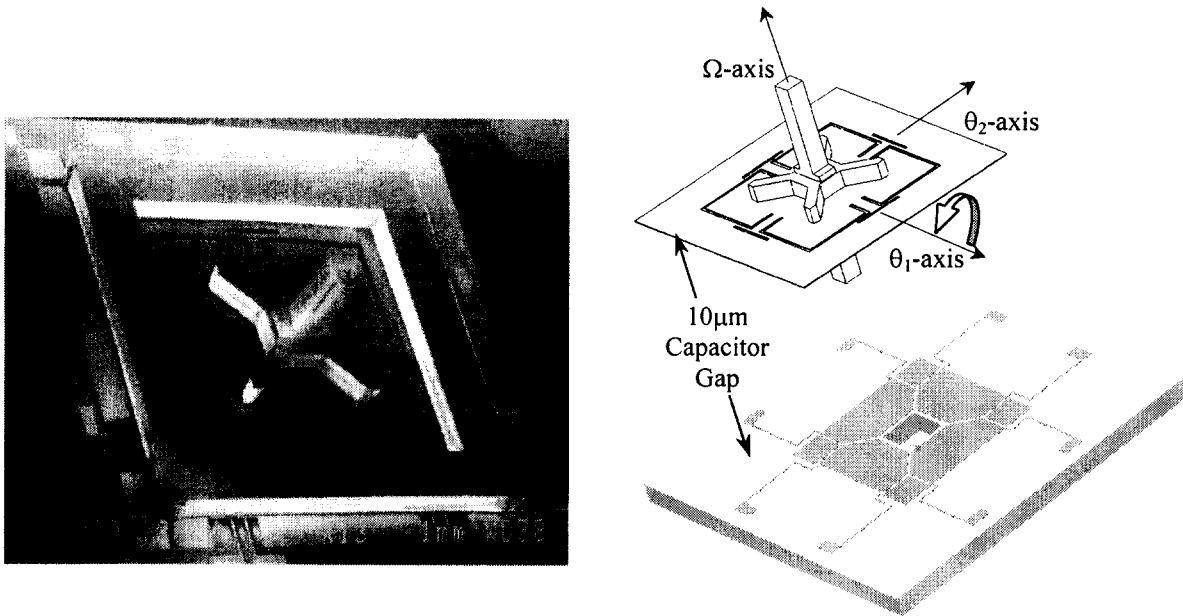


**Figure 1. (Left)** An SEM photo of a fabricated JPL MEMS micro-gyroscope  
**(Right)** A sketch of the micro-gyroscope’s cloverleaf (top) and electrode-plate (bottom)

Like all other Coriolis based sensors, JPL's gyroscope has 2 main vibratory degrees-of-freedom. This two degree-of-freedom system then exhibits two natural vibratory modes at frequencies  $f_1$  and  $f_2$ . In the perfect case, the symmetry of machining causes these frequencies to be the same (i.e. degenerate) however, manufacturing errors always ensure some degree of frequency mismatch and modal misalignment. Biasing the cloverleaf with a positive voltage, allows the electrodes in the electrode-plate to drive the cloverleaf into a rocking motion that is close in frequency and direction to one of the natural modes. This is the “drive axis”. Rotating the device around the  $\Omega$ -axis (i.e. the main sensor axis) causes some of this vibratory energy to be transferred into the other “sense” mode. This vibratory motion is picked up as a sinusoidally varying capacitance between the sense electrodes and the biased cloverleaf and is converted in to a voltage via a transimpedance amplifier. Synchronously demodulating this voltage signal with a sensed copy of the drive mode’s rock produces a baseband signal proportional to the inertial rate of the device along its  $\Omega$ -axis. In practice, the rocking motion in the drive direction is produced by an automatic gain control (AGC) loop which tracks the natural frequency of the gyroscope. Also, the energy transferred to the sense mode is damped electronically by a force rebalance (FRB) loop ensuring fast and stable rate response of the overall sensor system.

Observing figures 1 and 2 for electrode labels, pads  $C_1$  and  $C_2$  drive the cloverleaf's thin petal membrane for both the AGC and FRB loops. Pads  $S_2$ ,  $S_3$ , and  $S_4$  each are connected to transimpedance amplifiers and provide differential sensing of the two modes. The other pads,  $C_3$ ,  $C_4$ , and  $S_1$  are biased statically with respect to the resonator causing an effective softening of the spring matrix characterizing the device mechanics. A combination of static voltages on these pads can tune the natural modes of a resonator such that they are aligned with the preferred sensing and driving directions dictated by the electrode plate’s layout, and can further bring these aligned modes’ respective frequencies together such that there is maximal coupling of vibration between modes under rotation. (See Electrostatic Tuning Section)

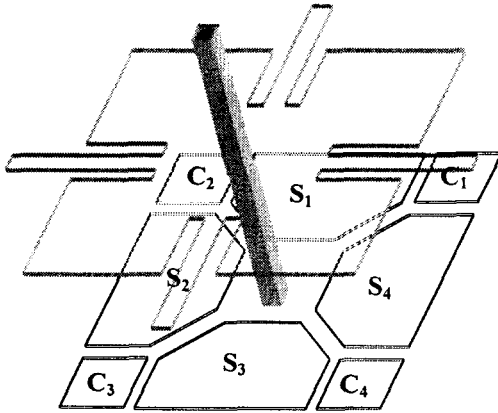


**Figure 2.** 8-Electrode layout. Cloverleaf drawn semi-transparently on top to visualize the electrodes' arrangement with respect to 4mm square side cloverleaf membrane.

- C<sub>1</sub>, C<sub>2</sub> : Driving electrodes
- S<sub>2</sub>, S<sub>3</sub>, S<sub>4</sub> : Sensing electrodes
- S<sub>1</sub>, C<sub>3</sub>, C<sub>4</sub> : Bias-Voltage applying (spring softening) electrodes

### Previous vs. Current Fabrications

#### Summary

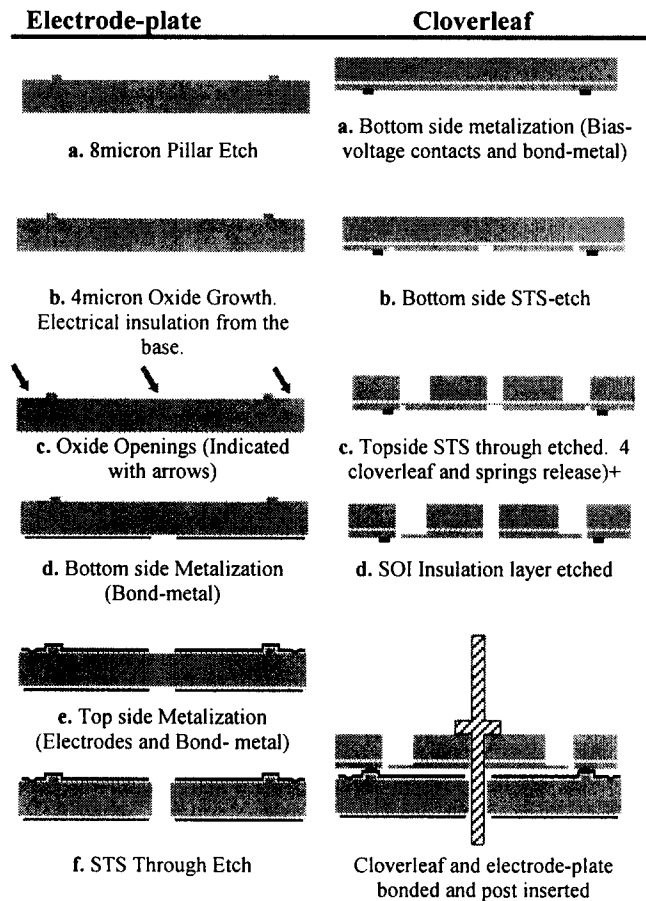
**Table 1.** Comparing previous and current fabrication methods.

Steps	Previously Fabricated		Current Fabricated	
	Method	Disadvantage	Method	Advantage
Cloverleaf's thin, inertial membrane etching	EDP	Springs and inertial membrane not precisely symmetric	STS DRIE	Springs and inertial membrane closely symmetric
Through-Etching	EDP	Long etching (~1 day), Asymmetric, Slanted side walls, Provides little grip for a post flange to bond	STS DRIE	Short etching (~3 hours), Symmetric, straight sidewalls, Provides maximum areas for a post flange to bond intimately (Observe Figure 1 left.)
Electrode-plate pillar etching	STS, RIE, Low temperature, 30% wt. KOH etching	Spikes in STS and Hillocks in KOH observed (See Appendix 1, comparison studies among STS, RIE's CF <sub>4</sub> /O <sub>2</sub> , and KOH etchings)	95 degree, 40% wt. KOH concentration etching	Uniform etch
Post material	Machined cylindrical metal	Thermally mismatched	Square Silicon post	Thermally matched
Capacitance gap between cloverleaf and electrode-plate	25 μm	Electronic noise, minimal tuning range	10 μm gap	Reduced noise, larger tuning capacity consequently from a smaller capacitance gap
Number of electrodes	4 electrodes	Limited electrostatic tuning	8 electrodes	Created linear-combinations of 3 electrode tuning
Packages	Honeywell's Accelerometer Package	Low Q	Ceramic Package	Higher Q

## Fabrications

Baseplate fabrication start with 500 $\mu$ m thick, 100mm diameter, 100 oriented, double side polished, and P-type doped wafer, having a resistance as low as 10 $\Omega$ -cm. Cloverleaf fabrication start with 26micron thin SOI, 500 $\mu$ m thick, 100mm diameter, double side polished, and p-type doped, a resistant as low as 10 $\Omega$ -cm wafers.

### Appendix 1. Comparisons among STS, RIE, and KOH



## Electrostatic Tuning

For optimal performance, the two modal frequencies of the resonator must be split in frequency by less than half the 3dB bandwidth of the mechanical resonance peaks, and these resonance peaks must have very high Q's and thus very narrow bandwidths. This requirement is extremely onerous for the standard MEMS manufacturing processes and would reduce yield (or performance) to unacceptable levels if other post-manufacture tuning techniques were not used. JPL has handled this potential dilemma in this way: First, we use manufacturing techniques that can natively (pre-tuning) achieve frequency splits on the order of 0.4% as shown in the following data table. Second, this still relatively large split can be completely compensated for using multi-degree-of-freedom electrostatic spring softening. Electrostatic spring softening is a well-known technique, which amounts to a form of "perfect" proportional feedback using the fact that the force between a capacitor's plates is a non-linear function of the distance between the plates. It is however a relatively weak effect in that in most designs it cannot fully compensate for manufacturing splits. The relatively large area provided by the JPL cloverleaf resonator along with the small gap size of 10um has been designed to ensure that tuning to degeneracy can be achieved using reasonable voltages.

Figure 3 demonstrates this electrostatic tuning ability of a JPL MEMS gyroscope. In the six gyros tested in the current experiments, we tuned the splits only to a point we deemed necessary to see optimal performance from the device under test. In another set of tests not shown, we pushed the tuning procedure to the limits of our measuring ability achieving a 10mHz split as tested by changing the rocking angle to many distinct directions and measuring the frequency that the AGC locked onto. Under these conditions, the resonator ceases to behave like a system with two preferential vibratory modes and displays a behavior very reminiscent of a Foucault pendulum, only with a much higher restoring stiffness (i.e. frequency).

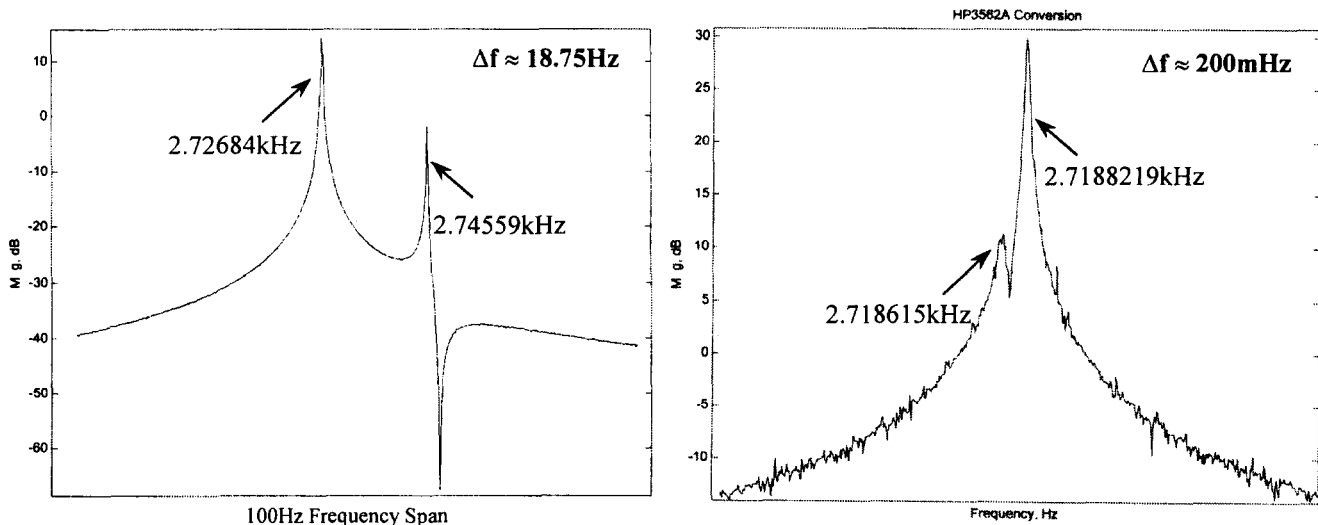


**Figure 3.** Micro-gyroscope #8 (Its result is further summarized in Table 2)  
(Left) Native frequency split at rocking mode,  $\Delta f \approx 18.75\text{Hz}$   
(Right) After applying electrostatic bias voltages on 3 of the 8 electrodes,  $\Delta f \approx 200\text{mHz}$

## Results

Six of the JPL's MEMS gyroscopes have been recently tested and are summarized in Table 2 below. Also, Honeywell Inc. had tested an additional one of the JPL's gyroscopes independently and reported its bias stability (flicker floor) to be 1 degree/hr.

**Table 2.** Test summary of 6 micro-gyroscopes from 3 different batches: B, C, and D (2nd column). Note the electrostatic tuning brought average 0.4% native frequency split to narrower average split of ~0.02%.

Gyro # Tested	Gyro Batch	Native Split (Hz)	Q (high)	Q (lower)	Split (Hz)	Performance (Degree/hour)
5	B	8.3	32,000	4,700	1.0	5
6	C	8.5	19,000	9,300	1.0	20
8	D	19	76,000	42,000	0.2	2
9	B	11	30,000	12,000	0.5	25
13	B	8.0	48,000	29,000	0.5	6
14	B	12	19,000	17,000	0.3	10
		11/1.8	37,000/ 9,700	19,000/ 6,300	0.6/ 0.15	11/ 4

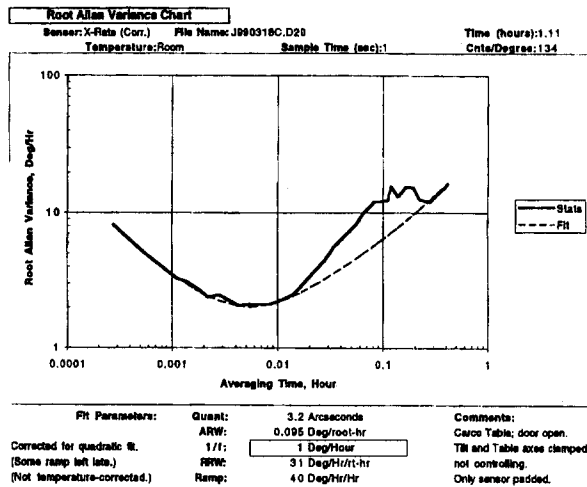


**Figure 4.** (Top left, top right, and bottom left )  
 Honeywell Inc. tested a JPL micro-gyroscope; their 3rd party test result shows bias instability (1/f floor fit) of 1degree/hour (boxed)  
 (Right bottom Picture)  
 Micro-gyro semi-packaged and staged on a zero-insertion socket

### Conclusion

No post-manufacturing mechanical trimming was done for the six tested microgyros in the table. Only electrostatic tuning was needed to achieve the performance listed. The JPL microgyro's design, with its intrinsic large electrodes, has made this possible. This ability appears favorable to high yield, mass production of high performing MEMS gyroscopes, eliminating the need for individualized mechanical trimming for high performance (at least for frequency splits). Also, the switch to STS RIE has added the precision needed to get into this electrostatic tuning range. We believe that the current manufacturing, tuning, and control procedures, and most importantly the overall cloverleaf design, is proceeding along the path necessary to allow mass production of high performance MEMS gyroscopes. Our current research directions are aimed at increasing the resonator Q, automating the electrostatic tuning procedure, and eliminating long-term drift sources through novel control techniques, all of which are designed to push performance further into the sub-1 degree/hr range.

## Appendix 1

Because the JPL MEMS gyroscope has large electrodes that are only  $10\mu\text{m}$  right beneath the resonating cloverleaf, a uniformly etched surface is crucial; any defect would stop the cloverleaf from vibrating vertically. See Table 1. Comparing among 3 available etching methods, KOH showed the best uniformity. RIE's uneven etch depth was too large to be implemented and STS left mysterious ring-spikes other than its unevenly etched surface. (See Figure 5)

**Table 3.** Comparisons of the three etching methods

	STS	RIE	KOH
Mask	$12\mu\text{m}$ PR	$12\mu\text{m}$ PR	5000A SiO <sub>2</sub>
Etch Rate	$2\mu\text{m}/\text{min}$	$0.5\mu\text{m}/\text{min}$	$0.6\mu\text{m}/\text{min}$
Etch Depth Uniformity (Ctr. to Edge)	$1.5\mu\text{m}$ Over $10\mu\text{m}$ depth	$2\mu\text{m}$	$< 0.5\mu\text{m}$
Sidewall Profile	Caved in	Curved out	Slanted
Problems	Leaves Defect	Large etch depth difference	Hillocks
Reference Figure	Figure 2 top & 3,	Figure 2 middle	Figure 2 bottom & 4,

### Uniformity Issue

STS-etching leaves defects on the surface. The defects are inherent to STS equipment when etching the thin depth  $< 20\mu\text{m}$ .

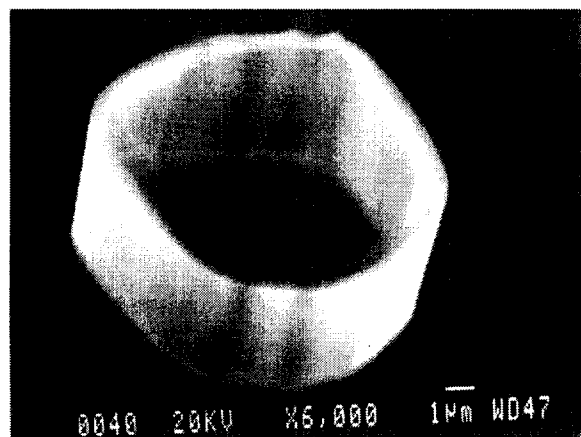
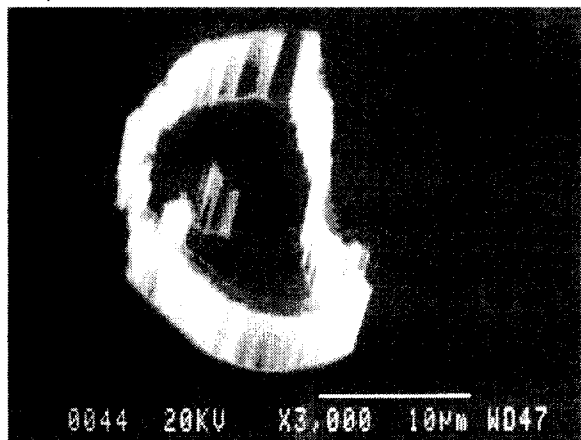


**Figure 5.** STS-etching leaves unwanted bumps that are virulent to the vertical resonator.

### Sidewall problem

When one needs continuous metal coverage over steps or pillars, a slanted sidewall is convenient. (Figure 6) Even though planetary evaporation could solve the problem, sometimes photoresist can not spin-coat over tall abrupt steps. STS DRIE's inherent etching quality in our case of creating pillars was not welcomed.

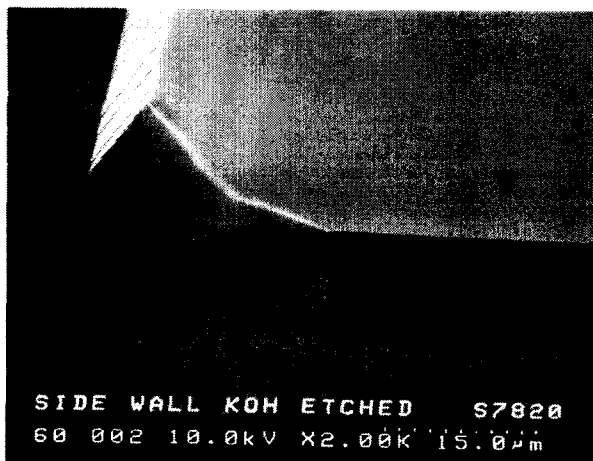
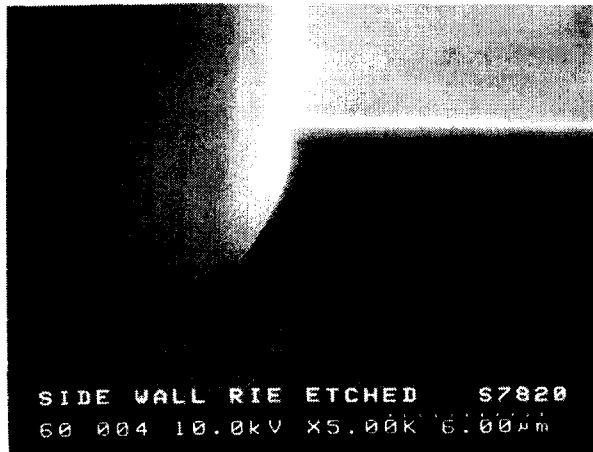
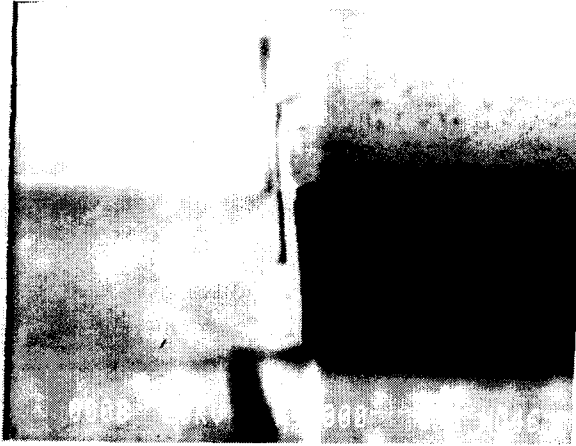


**Figure 6.** Top. STS etched. Note a caved sidewall  
Middle. RIE etched. Rather concaved sidewall  
Bottom. KOH etched. Angled sidewall

### Additional Problem: Hillocks

Upon choosing KOH etching method, JPL MEMS team learned the KOH-etching left hillocks when parameters were not set right (Figure 5). While striving to find optimal settings, we referred to Reference [4] and set 40% KOH wt. concentration at 95 Celsius degree temperature were most suitable to etch 10 $\mu$ m shallow depth. The etch rate was about 0.7micron/min.

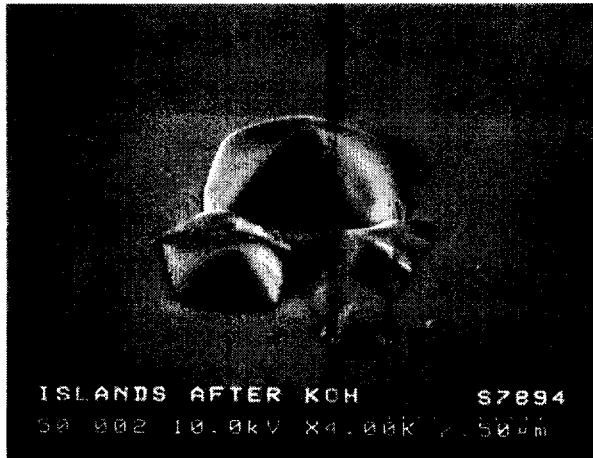


**Figure 5.** Hillocks happened at 30% wt. KOH concentration, 80 Celsius degree.

### References

- [1] T. K. Tang, R. C. Gutierrez, J. Wilcox, C. Stell, V. Vorperian, R. Calvet, W. Li, I. Charkaborty, R. Bartman, W. Kaiser, "Silicon Bulk Micromachined Vibratory Gyroscope", Tech Digest, Solid-State Sensor and Actuator Workshop, Hilton Head, S. C. pp. 288-293, June 1996.
- [2] T. K. Tang, R. C. Gutierrez, C. B. Stell, V. Vorperian, G. A. Arakaki, J. T. Rice, W. J. Li, I. Chakraborty, K. Shcheglov, J. Z. Wilcox, W. J. Kaiser, "A packaged silicon MEMS vibratory gyroscope for microspacecraft", in *Proc. IEEE Micro Electro Mechanical Systems Workshop (MEMS '97)*, Japan, 1997, pp. 500-505.
- [3] R. C. Gutierrez, T. K. Tang, C. B. Stell, V. Vorperian, K. Shcheglov, "Bulk Micromachined Vacuum Sensor," *Transducers 97, International Conference on Solid-State Sensors and Actuators, Digest of Technical Papers, 1997*, start pp. 1497.
- [4] H. Schroder, E. Obermeier, A. Steckenborn, "Micropyramidal hillocks on KOH etched {100} silicon surfaces: Formation, prevention, and removal," *Journal of Micromechanics and Microengineering*, pp. 139-145, June 1999.